

PSR J0210+5845; An ultra wide binary pulsar with a B6 V main-sequence star companion

E. van der Wateren^{1,2}, C. G. Bassa¹, G. H. Janssen^{1,2}, I. V. Yanes-Rizo^{3,4}, J. Casares^{3,4},
G. Nelemans^{2,5,6}, B. W. Stappers⁷, and C. M. Tan^{8,9,10}

¹ ASTRON, Netherlands Institute for Radio Astronomy, Oude Hoogeveensedijk 4, 7991 PD Dwingeloo, The Netherlands

² Department of Astrophysics/IMAPP, Radboud University Nijmegen, P.O. Box 9010, 6500 GL Nijmegen, The Netherlands

³ Instituto de Astrofísica de Canarias, E-38205 La Laguna, Tenerife, Spain

⁴ Departamento de Astrofísica, Universidad de La Laguna, E-38206 La Laguna, Tenerife, Spain

⁵ Institute of Astronomy, KU Leuven, Celestijnenlaan 200D, 3001 Leuven, Belgium

⁶ SRON, Netherlands Institute for Space Research, Niels Bohrweg 4, 2333 CA Leiden, The Netherlands

⁷ Jodrell Bank Centre for Astrophysics, Department of Physics and Astronomy, University of Manchester, Manchester M13 9PL, UK

⁸ Department of Physics, McGill University, 3600 rue University, Montréal, QC H3A 2T8, Canada

⁹ The Trottier Space Institute at McGill, 3550 rue University, Montréal, QC H3A 2A7, Canada

¹⁰ International Centre for Radio Astronomy Research, Curtin University, Bentley, WA 6102, Australia

Received December 5, 2023; accepted December 5, 2023

ABSTRACT

We report on radio timing observations of PSR J0210+5845 which reveal large deviations from typical pulsar spin-down behaviour. We interpret these deviations as being due to binary motion around the $V = 13.5$ star 2MASS J02105640+5845176, which is coincident in celestial position and distance with the pulsar. Archival observations and new optical spectroscopy identify this star as a B6 V star with a temperature of $T_{\text{eff}} \approx 14\,000$ K and a mass of $M_c = 3.5$ to $3.8 M_{\odot}$, making it the lowest mass main-sequence star known orbiting a non-recycled pulsar. We found that the timing observations constrain the binary orbit to be wide and moderately eccentric, with an orbital period of $P_b = 47^{+40}_{-14}$ yr and eccentricity $e = 0.46^{+0.10}_{-0.07}$. We predict that the next periastron passage will occur between 2030 and 2034. Due to the low companion mass, we find that the probability for a system with the properties of PSR J0210+5845 and its binary companion to survive the supernova is low. We show that a low velocity and fortuitously directed natal kick is required for the binary to remain bound during the supernova explosion, and argue that an electron-capture supernova is a plausible formation scenario for the pulsar.

Key words. stars: neutron – stars: binaries – pulsars: individual: PSR J0210+5845

1. Introduction

Within the population of about 3300 radio pulsars presently known (Manchester et al. 2005), there exists a distinct sub-population of six binary systems where a normal (non-recycled) pulsar, orbits a massive stellar companion. These binary systems have eccentric orbits with orbital periods on the order of months or years (Kaspi et al. 1996; Lorimer et al. 2006; Shannon et al. 2014) or even decades (Lyne et al. 2015). The secondary stars are O or B stars with masses exceeding $8 M_{\odot}$ (Bell et al. 1995; Lyne et al. 2015), and for those systems located in our Galaxy, they have low Galactic latitudes. Table 1 summarises the main properties of the six pulsar/massive star binaries known to date.

Most of the systems exhibit significant interaction between the pulsar and the stellar wind or disc of the massive stellar companion (Andersen et al. 2023), leading to variations in scattering and dispersion (Madsen et al. 2012), eclipses of the pulsar emission (Wang et al. 2004), and/or X-ray or gamma-ray emission (Aharonian et al. 2005). As a result, these systems serve as exceptional laboratories for investigating binary interactions in stellar disks and winds. They are thought to be possible progenitors of double neutron star systems (Johnston et al. 1994).

The progenitors of these pulsar/massive star binaries are systems composed of two massive main-sequence stars. In such systems, no stellar interaction is necessarily required, although it is possible that mass transfer has occurred in systems with small orbital periods. When the primary star undergoes supernova to form the neutron star, it sheds a large portion of its envelope (Matzner & McKee 1999). If a binary system loses more than half of its mass, the system is usually disrupted, because the orbital energy surpasses the binding energy (Hills 1983). Furthermore, asymmetries in the supernova explosion can impart a natal kick to the newborn neutron star, and depending on the velocity (speed and direction) of the kick with respect to the orbital velocity, the binary binding energy can be further altered, possibly counteracting the disruption of the binary or vice versa. In those cases where the binary remains bound, the neutron star will orbit the unaltered massive main-sequence star in a wide orbit with high eccentricity (e.g. Brandt & Podsiadlowski 1995).

In 2017, PSR J0210+5845 was discovered as part of the LO-FAR Tied-Array All-Sky Survey (LOTAAS), the LOFAR pulsar survey of the northern hemisphere (Sanidas et al. 2019). Tan et al. (2020) showed that initial timing observations revealed significant timing residuals that they argue could be caused by timing noise intrinsic to the pulsar. In this study, we show that the

timing residuals are the result of binary motion with an $M_c = 3.5$ to $3.8 M_\odot$ companion in a moderately eccentric, long period orbit. The PSR J0210+5845 system has the lowest-mass binary companion among known pulsar/massive star binaries, posing a challenge for its survival of the supernova explosion that formed the neutron star.

We present continued timing observations in Section 2 that show that the spindown of PSR J0210+5845 can be modelled by several higher-order spin-frequency derivatives. We find that a $V \sim 13.5$ star is coincident with the pulsar timing position, discuss its properties as the optical counterpart to PSR J0210+5845, and identify it as the binary companion of the pulsar in Section 3. In Section 4, we use the spin frequency derivatives to obtain orbital constraints and investigate formation scenarios in Section 5. We discuss and conclude in Section 6.

2. Radio timing

The timing ephemeris of PSR J0210+5845 obtained by Tan et al. (2020), modelling the position, the spin period and its derivative, and the dispersion measure (DM), uses LOFAR observations obtained between December 2017 and December 2018. We extended that timing ephemeris with observations from 2019 to June 2022. All observations of PSR J0210+5845 were obtained with the same observational setup. We used the high-band antennas (HBAs) of the LOFAR core stations, recording dual-polarisation Nyquist sampled complex voltages for 400 subbands of 0.195 MHz bandwidth between 110 to 188 MHz. We followed the analysis procedure outlined in van der Wateren et al. (2023), where we used the LOFAR pulsar pipeline (Kondratiev et al. 2016) to coherently dedisperse and fold the observations with DSPSR (van Straten & Bailes 2011) to create pulse profiles in the PSRFITS¹ format with 0.195 MHz channels and 5-s subintegrations. The majority of radio frequency interference (RFI) was automatically removed using CLFD² (Morello et al. 2019), followed by a manual inspection and RFI removal with the PSRZAP tool from the PSRCHIVE software suite (Hotan et al. 2004) where needed.

We used the timing model from Tan et al. (2020) to fold and dedisperse all observations, which were then fully averaged in time. To obtain a better constraint on the DM, the observations were split into two subbands with centre frequencies 129 and 167 MHz and both subbands were fully averaged in frequency. We combined the observations to one high signal-to-noise profile of the full bandwidth, to which we modelled an analytical template profile as the sum of three von Mises functions using PAAS. The averaged observations were cross-correlated with the template to obtain times-of-arrival (TOAs) with PAT.

With PINTK, the interactive module of the pulsar timing package PINT³ (Luo et al. 2021) (v0.9.3), a new timing ephemeris was constructed modelling the celestial position (α_{J2000} , δ_{J2000}), spin frequency f , spin frequency derivative \dot{f} , and the DM. As indicative in Fig. 1, higher-order spin frequency derivatives were required to properly model the spindown behaviour of PSR J0210+5845. We sequentially added spin frequency derivatives beyond \dot{f} to improve the timing ephemeris and obtained significant measurements for the second, third, and fourth spin frequency derivatives \ddot{f} , $\ddot{\dot{f}}$, and $\ddot{\ddot{f}}$. Fitting a timing ephemeris that also included a fifth spin frequency derivative in the fit resulted in a value that was not significant (less than 3σ significance).

¹ <https://psrchive.sourceforge.net>

² <https://github.com/v-morello/clfd>

³ <https://nanograv-pint.readthedocs.io/en/latest>

To assess the timing noise using the method from Arzoumanian et al. (1994), we fitted f , \dot{f} , and \ddot{f} , keeping higher-order frequency derivatives at zero, over a 10^8 -s segment of the data to calculate $\Delta_8 = \log_{10} \left((6f)^{-1} |\ddot{f}| t^3 \right)$, with $t = 10^8$ s. The obtained value of $\Delta_8 = 1.54$ significantly exceeds the expected value for intrinsic timing noise of $\Delta_8 = -1.3$ based on the relation from Hobbs et al. (2010), which suggests that the higher-order frequency derivatives are not primarily produced by intrinsic timing noise.

The higher-order spin frequency derivatives up to and including the fifth spin frequency derivative were included in the timing ephemeris. Even though the fifth spin frequency derivative was not significant, it was included due to the informative nature of its uncertainty, particularly in terms of the scale for this parameter, which was used in Section 4. The timing model was subsequently refitted for all parameters, resulting in the timing ephemeris shown in Table 2 and the timing residuals in Fig. 1.

To check that there are no unexpected covariances between the parameters in the timing ephemeris, we performed a Bayesian analysis using the Markov Chain Monte Carlo (MCMC) fitter from PINT. The standard PINT approach was used by taking normally distributed priors based on the standard PINT fitting results and refitting all parameters in the timing ephemeris using the MCMC fitter. The parameters and their uncertainties are consistent between fitting methods, and covariances are generally low except for pairs of odd and even spin frequency derivatives, as expected for a Taylor series.

To investigate for variations in dispersion, we divided the TOAs into segments, each spanning 200 days, which we independently refitted for DM. This analysis revealed a maximum variation of $0.38(49) \text{ pc cm}^{-3}$, with the uncertainty denoting the average error associated with the separately fitted DMs. Refitting the full data set for a time derivative of the DM resulted in $\dot{\text{DM}} = -0.0006(15) \text{ pc cm}^{-3} \text{ yr}^{-1}$. Hence, we conclude that PSR J0210+5845 exhibits no significant DM variations in our dataset.

Coincident with the timing position of PSR J0210+5845 is an optical star for which the position and proper motions are documented in the *Gaia* DR3 catalogue (Gaia Collaboration et al. 2023) and which, in Section 3, we identify as the binary companion of the pulsar. We refitted the spin frequency, higher-order derivatives of the spin frequency and the DM, incorporating the position and proper motions from the optical counterpart of PSR J0210+5845 as documented in the *Gaia* DR3 catalogue (Gaia Collaboration et al. 2023). The resulting timing model remained consistent with the model in which the position was fitted and no proper motion was assumed. See Section 3 for more information on the optical counterpart.

3. Optical counterpart

A star ($V = 13.5$, $B - V = 0.47$; Henden et al. 2015) is located near the radio timing position of PSR J0210+5845. This star is present in many catalogues – for the remainder of the paper, we will refer to it as 2MASS J02105640+5845176 (Skrutskie et al. 2006). The *Gaia* DR3 (Gaia Collaboration et al. 2023) astrometric solution provides a proper motion of $\mu_\alpha \cos \delta = -1.116(12) \text{ mas yr}^{-1}$ and $\mu_\delta = -0.495(15) \text{ mas yr}^{-1}$. At the epoch of the pulsar timing ephemeris, the position of this star is $\alpha_{\text{ICRS}} = 02^{\text{h}}10^{\text{m}}56^{\text{s}}.4094$, $\delta_{\text{ICRS}} = +58^\circ45'17''.716$. This position is offset from the pulsar timing position by $\Delta\alpha = 0''.06(7)$ in right ascension and $\Delta\delta = 0''.02(8)$ in declination and hence coincident with the pulsar position as measured through timing.

PSR name	P (s)	P_b (d)	e	M_c (M_\odot)	l	b	Ref.
J0045–7319	0.926	51	0.81	8.8	303°51	–43°80*	[1, 2]
B1259–63	0.048	1237	0.87	20	304°18	–0°99	[3, 4]
J1638–4725	0.764	1941	0.96	8 [†]	337°36	–0°30	[5]
J1740–3052	0.570	231	0.58	20	357°81	–0°13	[6, 7]
J2032+4127	0.143	16835	0.96	15	80°22	+1°03	[8]
J2108+4516	0.577	269	0.09	17.5 – 23	87°34	–1°63	[9]

Table 1. The six currently known pulsar/massive star binaries and their spin period (P), orbital period (P_b), eccentricity (e), companion mass (M_c), Galactic longitude (l) and latitude (b). The references used are: [1] Kaspi et al. (1996), [2] Bell et al. (1995), [3] Shannon et al. (2014), [4] Johnston et al. (1994), [5] Lorimer et al. (2006), [6] Bassa et al. (2011), [7] Madsen et al. (2012), [8] Lyne et al. (2015), and [9] Andersen et al. (2023). * PSR J0045–7319 is located in the Small Magellanic Cloud, hence the large Galactic latitude. [†] The companion of J1638–4725 has not been identified. The mass estimate is the median mass calculated from the orbital period and projected-semi major axis, assuming an inclination of 60°.

Table 2. The timing parameters for PSR J0210+5845. Two timing ephemerides are fitted, one where the celestial position is fitted together with five spin frequency derivatives and the dispersion measure, and one where the celestial position and proper motions are fixed to those of *Gaia* DR3. The *Gaia* positions are consistent with the positions from radio timing at the same epoch of position measurement. The higher-order frequency derivatives and DMs are consistent at the epoch of frequency determination. The figures in parentheses are the nominal 1σ uncertainties in the least significant digits quoted, which have been multiplied by the square root of the reduced χ^2 .

Data set and assumptions		
MJD range	58118–59704	
Data span (yr)	4.34	
Number of TOAs	110	
Clock correction procedure	TT(TAI)	
Solar system ephemeris model	DE436	
Units	TDB	
Measured quantities		
	Fitting for astrometry	<i>Gaia</i> DR3 astrometry
Epoch of position measurement (MJD)	58910.0	57388.5
Right ascension, α_{J2000}	02 ^h 10 ^m 56 ^s .416(9)	02 ^h 10 ^m 56 ^s .409999
Declination, δ_{J2000}	+58°45′17″.74(8)	+58°45′17″.718237
Proper motion in RA, $\mu_\alpha \cos \delta$ (mas yr ^{–1})	...	–1.116
Proper motion in Dec., μ_δ (mas yr ^{–1})	...	–0.495
Epoch of frequency determination (MJD)	58910.0	58910.0
Spin frequency, f (s ^{–1})	0.566181225686(6)	0.566181225686(6)
First derivative of spin frequency, \dot{f} (s ^{–2})	–4.86224(6)×10 ^{–14}	–4.86223(6)×10 ^{–14}
Second derivative of spin frequency, \ddot{f} (s ^{–3})	–1.1628(3)×10 ^{–22}	–1.1628(3)×10 ^{–22}
Third derivative of spin frequency, \dddot{f} (s ^{–4})	–4.96(4)×10 ^{–31}	–4.96(4)×10 ^{–31}
Fourth derivative of spin frequency, $\overset{\cdot\cdot\cdot}{f}$ (s ^{–5})	–2.47(13)×10 ^{–39}	–2.47(12)×10 ^{–39}
Fifth derivative of spin frequency, $\overset{\cdot\cdot\cdot\cdot}{f}$ (s ^{–6})	–1.9(2.0)×10 ^{–47}	–1.5(1.9)×10 ^{–47}
Dispersion measure, DM (pc cm ^{–3})	76.7895(18)	76.7894(18)
Weighted rms timing residual (μ s)	860.7	864.5
Reduced χ^2 value	0.89	0.90

The parallax of this star has been measured at $\varpi = 0.354(15)$ mas in *Gaia* DR3. The *Gaia* GSP-Phot and FLAME modelling combine this parallax with GAIA photometry and stellar models to estimate a distance of $d = 2.21$ kpc, a nominal effective temperature of $T_{\text{eff}} = 10930$ K, and a mass of $M_c = 3.10 M_\odot$ (Gaia Collaboration et al. 2023). Similar stellar properties were obtained with the StarHorse Bayesian isochrone-fitting software (Queiroz et al. 2018) by combining the GAIA astrometric and photometric measurements with photometry from Pan-STARRS1, 2MASS, and AllWISE. Results based on *Gaia* DR2 are presented in Anders et al. (2019) and updated using *Gaia* EDR3 in Anders et al. (2022). These results are shown in Table 3.

Low-resolution spectroscopy of 2MASS J02105640+5845176 has been obtained as part of the LAMOST survey, which initially classified the star as an

A1 V star and estimates a radial velocity of $-7.6(5)$ km s^{–1} (Xiang et al. 2022). Stellar parameters derived from this spectrum vary between analysis methods, with $T_{\text{eff}} = 7840(253)$ K obtained by Xiang et al. (2019) from LAMOST DR5 and $T_{\text{eff}} = 14279(603)$ K by Xiang et al. (2022) from LAMOST DR6. Queiroz et al. (2020) used the LAMOST DR5 stellar parameters for the lower effective temperature solution from Xiang et al. (2019) with the StarHorse software to obtain lower mass and distance estimates of 2MASS J02105640+5845176 ($d = 1.95$ kpc, $M_c = 1.69 M_\odot$) compared to the photometric results (see Table 3). The higher effective temperature obtained in Xiang et al. (2022) is consistent with the mass and temperature estimates derived from astrometry and photometry.

To resolve this discrepancy in the effective temperature of 2MASS J02105640+5845176, we obtained four spectroscopic observations of 2MASS J02105640+5845176 during morning

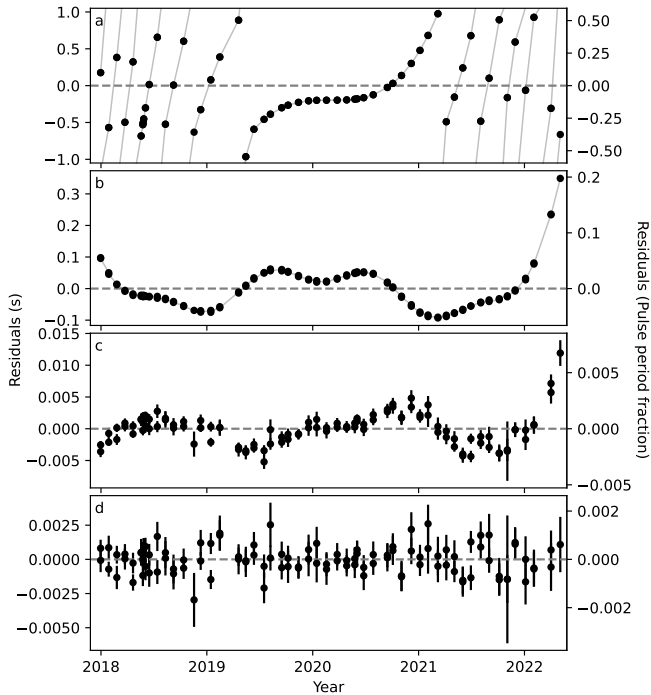


Fig. 1. The residuals from timing with one (a), two (b) three (c), and four (d) spin frequency derivatives. The residuals from fitting the model in Table 2 fitting up to and including five spin frequency derivatives are very similar to the residuals shown here.

d (kpc)	M_c (M_\odot)	T_{eff} (K)	Ref.
2.5(5)*	-	-	Cordes & Lazio (2002)
2.0(4)*	-	-	Yao et al. (2017)
2.31 ^{+0.27} _{-0.20}	2.78 ^{+0.48} _{-0.83}	11 457 ⁺⁹⁷² ₋₄₂₉₈	Anders et al. (2019)
-	-	7840(253)	Xiang et al. (2019)
1.95 ^{+0.04} _{-0.07}	1.69 ^{+0.10} _{-0.04}	8261 ⁺²⁸⁵ ₋₉₄	Queiroz et al. (2020)
2.60 ^{+0.11} _{-0.10}	-	-	Bailer-Jones et al. (2021)
2.51 ^{+0.05} _{-0.14}	3.22 ^{+0.40} _{-0.62}	12 260 ⁺¹⁴⁰⁸ ₋₁₃₁₁	Anders et al. (2022)
2.2070 ^{+0.0042} _{-0.0011}	3.10 ^{+0.07} _{-0.05}	10 930 ⁺⁵ ₋₂₈	Gaia Collaboration et al. (2023)
-	-	14 279(603)	Xiang et al. (2022)
-	3.5 to 3.8	14275(133)	This paper

Table 3. The distance d , mass M_c , and effective temperature T_{eff} of 2MASS J02105640+584517 as documented in different catalogues. The uncertainties are 68% confidence intervals as upper and lower bounds or 1σ uncertainties in parentheses. Distances denoted with * are derived from the location and DM of the pulsar using the NE2001 (Cordes & Lazio 2002) and YMW16 (Yao et al. 2017) Galactic electron density models.

twilight on August 16 and 17, 2022 with the Intermediate Dispersion Spectrograph (IDS) at the 2.5 m Isaac Newton Telescope on La Palma. The R900V grating was used with 600-s exposures on the RED+2 detector. The seeing varied between $1''.3$ and $2''.1$. We used the $0''.974$ slit, covering the wavelength range of 3800 to 5400 Å at 0.70 Å pix^{-1} , providing a resolution of $R \sim 3000$. The observations were bias subtracted and spectra were extracted using the method described by Hynes (2002). Arc-lamp exposures taken prior to each observation of 2MASS J02105640+5845176

were used for the wavelength calibration. Radial velocities and spectral properties were determined by fitting the observed spectra against normalised model spectra from Munari et al. (2005). The model spectra were convolved with a truncated Gaussian to decrease their resolution of $R = 20\,000$ to that of the observations.

We found that the barycentred radial velocities are consistent with a mean velocity of $v = -9(3) \text{ km s}^{-1}$ (3.2 km s^{-1} rms around the mean). The observed spectrum is best represented by the models with Solar metallicity ($[M/H] = 0$) with an effective temperature $T_{\text{eff}} = 14\,275(133) \text{ K}$, surface gravity $\log(g/cgs) > 4.13$ (2σ) and rotationally broadened by $v_{\text{rot}} \sin i = 73(12) \text{ km s}^{-1}$. At this effective temperature and surface gravity, 2MASS J02105640+5845176 can be classified as a B6 V star (Pecaut & Mamajek 2013).

The PARSEC stellar evolution models by Bressan et al. (2012); Tang et al. (2014) and Chen et al. (2014, 2015) predict a mass of $M_c = 3.59(5) M_\odot$ and absolute V-band magnitude of $M_V = 0.28(4)$ for an $[M/H] = 0$ main-sequence star with $T_{\text{eff}} = 14\,275(133) \text{ K}$ at an age of 10 Myr. At 40 Myr, the mass and absolute V-band magnitude are $M_c = 3.72(6) M_\odot$ and $M_V = 0.06(4)$. The Green et al. (2019) Galactic extinction map predicts $E_{g-r} = 0.38(2)$ to $0.40(2)$ mag for distances from 1.9 to 3.0 kpc. For these reddening values, the $R_V = 3.1$ extinction coefficients from Schlafly & Finkbeiner (2011) yield $A_V = 1.15$ to 1.21 mag. Combined with the observed magnitude of $V = 13.507$ (Henden et al. 2015) this yields distances of $d = 2.54$ kpc to 2.80 kpc. From these observations, we conclude that the A1 V stellar classification and the $T_{\text{eff}} = 7840 \text{ K}$ estimate by Xiang et al. (2019) is in error and that 2MASS J02105640+5845176 is a $M_c = 3.5$ to $3.8 M_\odot$, $T_{\text{eff}} \sim 14\,000 \text{ K}$ B6 V star at a distance of $d = 2.5$ to 2.8 kpc.

At the location and DM of PSR J0210+5845, the NE2001 (Cordes & Lazio 2002) and YMW16 (Yao et al. 2017) Galactic electron density models predict distances of 2.52 and 1.95 kpc, respectively. Given the typically 20% uncertainties on DM-derived distances, these distances are consistent with the distances derived from the *Gaia* parallax measurement and the photometric and spectroscopic constraints.

The uncertainty in the tie between the pulsar position and the *Gaia* astrometry is dominated by the uncertainty in the former. The 99% confidence error ellipse on the pulsar timing position has an area of 0.053 sq. arcsec, while the *Gaia* DR3 object density towards PSR J0210+5854 is only 18.4 stars per sq. arcmin. Hence, the probability of finding an unrelated star from the *Gaia* DR3 catalogue in the error ellipse of PSR J0210+5854 is low $p = 2.6 \times 10^{-4}$. Given this low chance coincidence, and the consistent distance estimates, we will consider the optical counterpart 2MASS J02105640+5845176 as the binary companion to PSR J0210+5854 for the remainder of the paper.

Finally, we note that based on light curves from ZTF Bellm et al. (2019), Chen et al. (2020) identified 2MASS J02105640+5845176 as a periodic variable, with 0.042 mag variations in r -band on a 1.1248 d period, and classified it as a variable of the RS CVn type. This classification is inconsistent with the spectral type obtained from spectroscopy and the mass and temperature estimates from astrometry and photometry. Additionally, our optical spectroscopy rules out radial velocity variations larger than 3 km s^{-1} over a 24 h period, ruling out the RS CVn classification. We consider it more likely that 2MASS J02105640+5845176 is a slowly pulsating B-star, a variable type that produces photometric variability of similar periodicity and amplitude in stars of spectral types ranging from B2 to B9 (Waelkens 1991; Fedurco et al. 2020).

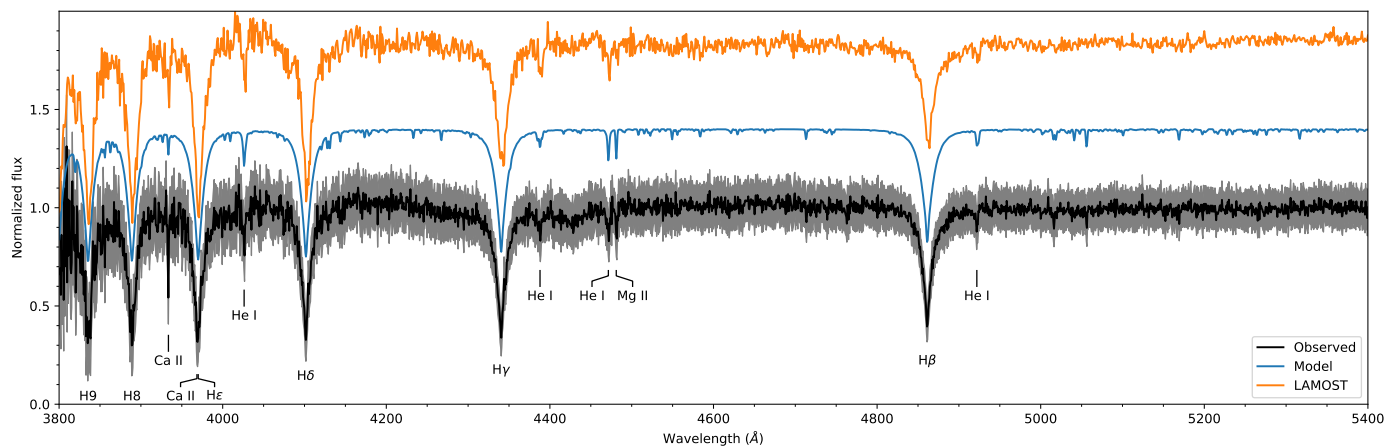


Fig. 2. The normalised optical spectrum of 2MASS J02105640+5845176 (black) as observed with the Intermediate Dispersion Spectrograph at the Isaac Newton Telescope. The best fitting model spectrum from [Munari et al. \(2005\)](#) is plotted in blue (shifted by +0.4 units vertically) and has $T_{\text{eff}} = 14\,000$ K, $\log g = 4.5$ cgs, $[M/H] = 0$ and $v_{\text{rot}} \sin i = 75$ km s $^{-1}$. The model spectrum has been convolved with the response of the slit to match the resolution of the observed spectrum. The LAMOST DR7 spectrum from [Xiang et al. \(2022\)](#) is shown in orange (shifted by +0.8 units vertically). Prominent absorption lines are indicated.

4. Orbital constraints

To investigate if binary motion between PSR J0210+5845 and 2MASS J02105640+5845176 can explain the observed higher-order spin frequency derivatives in the timing of PSR J0210+5845, we used the method from [Bassa et al. \(2016\)](#). This method is based on the derivations of [Joshi & Rasio \(1997\)](#) and uses a Keplerian orbit to compute time derivatives of the line-of-sight position of the pulsar to predict spin frequency derivatives. We consider it unlikely that PSR J0210+5845 and 2MASS J02105640+5845176 are in an unbound, hyperbolic, orbit, as the time scale for gravitational interaction will be extremely short compared to the lifetime of the pulsar. Hence, we modelled the observed spin frequency derivatives with a bound Keplerian orbit described by the orbital period P_b , projected semi-major axis x , eccentricity e , argument of perigee ω , and true anomaly ν .

For comparison of the observed spin frequency derivatives with predicted values from the Keplerian model, we used the first to fifth spin frequency derivatives. We implicitly assumed that the second and higher-order spin frequency derivatives are entirely dominated by orbital motion, but need to correct the observed first-order spin frequency derivative \dot{f}_{obs} for the unknown intrinsic spin frequency derivative \dot{f}_{int} due to spin down. The contributions to \dot{f}_{obs} from the Shklovskii ([Shklovskii 1970](#)) effect and the differential and Galactic acceleration (e.g. [Nice & Taylor 1995](#)) are at least six orders of magnitude smaller than \dot{f}_{obs} and are therefore neglected. From the ATNF Pulsar Catalogue⁴ (version 1.67, [Manchester et al. 2005](#)), we found that the intrinsic spin frequency derivative distribution of normal, non-recycled pulsars (those with spin period $P > 0.02$ s) can be described by a log-normal distribution of the form $\log_{10} -\dot{f}_{\text{int}} = -14.3(1.3)$ (for \dot{f}_{int} in units of s $^{-2}$).

We performed a Monte Carlo simulation to predict spin frequency derivatives for 100 000 randomly sampled Keplerian orbits. Samples of e , ω , and ν were drawn from uniform distributions between $0 \leq e < 1$, $0^\circ \leq \omega < 360^\circ$, and $0^\circ \leq \nu < 360^\circ$, respectively. Using the drawn samples, we used the equations from [Bassa et al. \(2016\)](#) and solved for P_b and x . Random values for the intrinsic spin frequency derivative \dot{f}_{int} were drawn from the

log-normal distribution to correct the observed spin frequency derivative and obtain the contribution due to orbital motion on \dot{f} . For each set of parameters, we calculated the spin frequency derivatives, which we compared to the observed values from the timing analysis in Section 2. We only retained parameter sets for which the predicted spin frequency derivatives were within 3σ of the observed values and for which the orbital inclination i was consistent with $\sin i < 1$ for a $1.4 M_\odot$ pulsar and a $M_c = 3.6 M_\odot$ binary companion.

The results of the Monte Carlo simulation are presented in Fig. 3 and they indicate that the observed spin frequency derivatives can be explained by a wide and moderately eccentric orbit with $P_b = 47^{+40}_{-14}$ yr, $x = 12.9^{+7.5}_{-5.2}$ AU and $e = 0.46^{+0.10}_{-0.07}$ (68% confidence intervals). The orbital inclination is constrained to $i = 52(18)^\circ$ and with a true anomaly of $\nu \sim 221^\circ$, the binary system had its previous apastron passage between 1988 and 2016 ($T_{\text{ap}} = 2009^{+7}_{-20}$) while the next periastron passage is predicted to occur between 2030 and 2034 ($T_{\text{per}} = 2032.1^{+1.7}_{-1.3}$). At periastron, the distance between the binary components will be $q = 11.7^{+5.0}_{-1.5}$ AU. By correcting for the orbital motion of PSR J0210+5845, we obtained an intrinsic spin-down $\dot{f}_{\text{int}} = -0.6^{+1.7}_{-0.5} \times 10^{-14}$ s $^{-2}$, constraining the characteristic age to $\tau_c = 1.6^{+13}_{-1.1}$ Myr.

If we assume a lower companion mass of $1.7 M_\odot$, we obtain a very similar estimate for ν and slightly lower estimates for P_b , x , e , ω , and \dot{f}_{int} , but the values are consistent with those from $M_c = 3.6 M_\odot$.

5. Formation scenarios

The formation of high-mass binary pulsars follows that of high-mass X-ray binaries and the first-born neutron star in double neutron star systems, where the more massive primary of a binary consisting of O and/or B stars undergoes a supernova explosion to form the neutron star (e.g. [Brandt & Podsiadlowski 1995](#); [Tauris et al. 2017](#), and references therein). Alternatively, an episode of mass transfer from the primary to the secondary can lead the primary to expel most of its envelope, leaving a Helium star that can explode as a Type Ib/c supernova ([Eldridge et al. 2008](#)).

PSR J0210+5845 poses a challenge for these formation scenarios as, compared to other high-mass binary pulsars, it

⁴ <http://www.atnf.csiro.au/research/pulsar/psrcat>

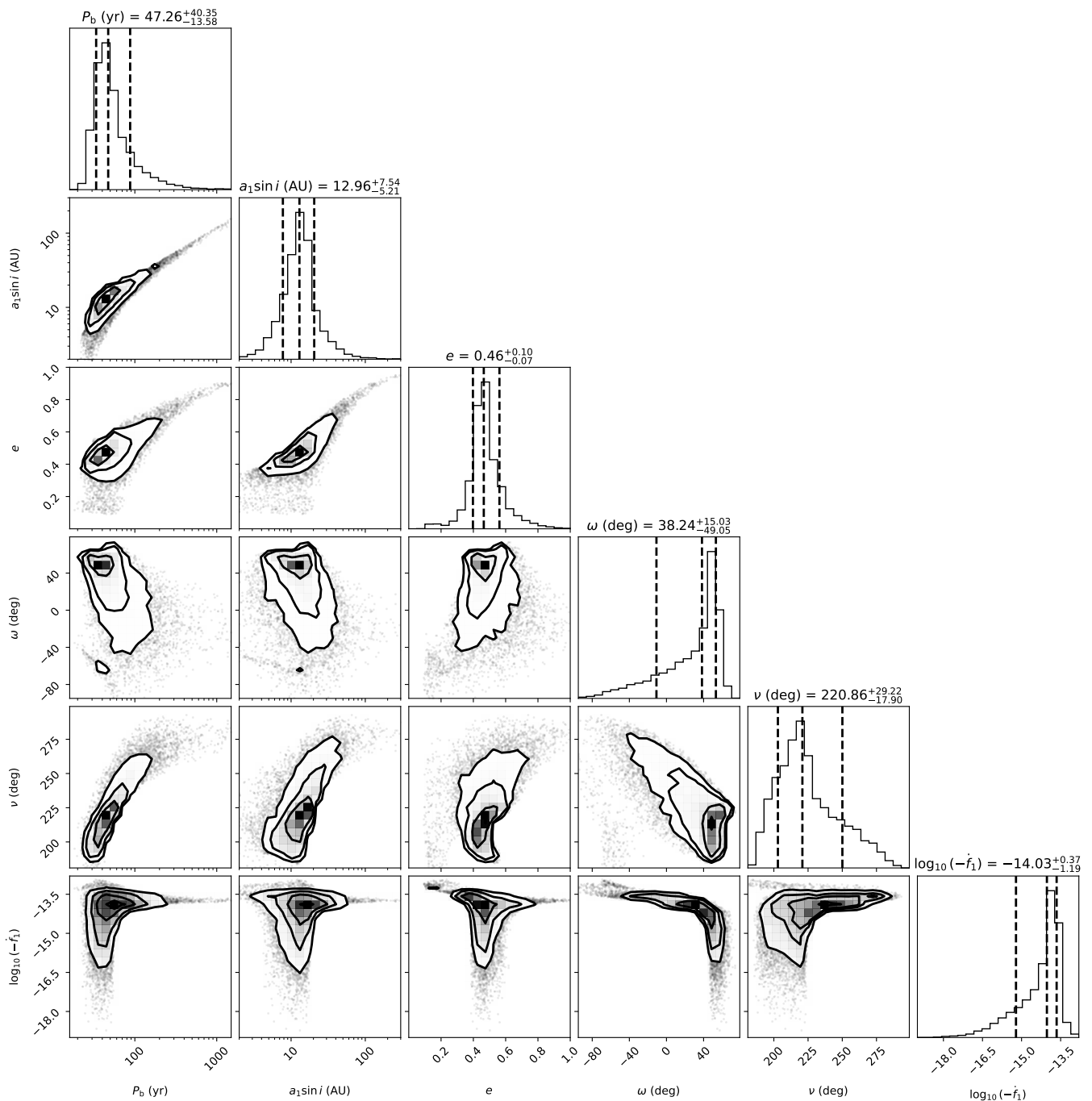


Fig. 3. The parameter distributions of the orbital period (P_b), the projected semi-major axis (x), the eccentricity (e), the argument of perigee (ω), the true anomaly (ν), and the intrinsic spin frequency derivative (f_{int}) resulting from the Monte Carlo simulation assuming $M_c = 3.6 M_\odot$. The median values and the 68% confidence intervals for each parameter are displayed on top of the columns.

has a relatively low companion mass of $\sim 3.6 M_\odot$. Since, in the absence of mass transfer, the progenitor of the pulsar in PSR J0210+5845 must have had a mass larger than $\geq 8 M_\odot$ to form a $\sim 1.4 M_\odot$ neutron star (Woolsey et al. 2002), at least 56% of the mass in the binary system would have been lost in a direct supernova explosion. As this exceeds the 50% limit above which the binary is disrupted (Hills 1983), a natal kick imparted on the neutron star during the supernova explosion would be required to keep the binary system bound.

To investigate the kick velocities required for the system to survive the mass loss in the supernova explosion, we used the

formalism by Brandt & Podsiadlowski (1995) to calculate post-supernova orbits. As input for the direct supernova channel, we assumed as initial conditions a $M_p = 8$ to $12 M_\odot$ neutron star progenitor and a $M_c = 3.6 M_\odot$ secondary in a wide orbit (initial orbital periods larger than $P_{b,\text{ini}} > 1500$ d) to ensure it does not fill its Roche lobe before the star explodes (Klencki et al. 2022). We assumed that the initial orbit is circularised due to tides from the neutron star progenitor. For these parameters, the Brandt & Podsiadlowski (1995) equations predict a maximum kick velocity of $v_{\text{kick}} < 96 \text{ km s}^{-1}$, above which the system will not remain bound. Hence, random kick velocities were chosen with magni-

tudes up to this limit and we used the standard assumption that the distribution in kick directions is isotropic.

We found that the orbit only remains bound for kicks with magnitudes below $v_{\text{kick}} < 96 \text{ km s}^{-1}$ and only if the kick direction is retrograde, i.e. opposite to the orbital velocity at the time of the supernova explosion. The kick velocity limit for which the system remains bound decreases as the initial orbit is wider, and has $v_{\text{kick}} < 37 \text{ km s}^{-1}$ for $P_{\text{b,ini}} = 16\,000 \text{ d}$, see Fig. 4. The fraction of cases that remain bound (assuming isotropic kicks) is relatively low and decreases for higher progenitor masses. Similarly, the probability for the system to remain bound improves for the alternative scenario where mass is lost from the system to form a Helium star. Repeating the calculations with a $M_{\text{p}} = 2.4$ to $4 M_{\odot}$ Helium star progenitor for the neutron star in a $P_{\text{b,ini}} > 1000 \text{ d}$ pre-explosion orbit, the calculations show that the binary system remains bound for retrograde kicks with velocities below $v_{\text{kick}} < 90 \text{ km s}^{-1}$, but the probability increases to 100% for velocities below $v_{\text{kick}} < 11 \text{ km s}^{-1}$, where also prograde orbits are possible.

If we consider a scenario with a less massive companion, the likelihood of the binary system surviving the supernova diminishes even further. Lower initial natal kicks to the neutron star are necessary to prevent disruption of the binary system.

The post-supernova orbits have a large range in possible orbital periods and eccentricities. Orbits that are initially wide are able to reproduce the observed orbital parameters determined with the spin frequency derivatives ($P_{\text{b}} = 47^{+40}_{-14} \text{ yr}$, $e = 0.46^{+0.10}_{-0.07}$). The post-supernova orbital period does not strongly depend on the progenitor mass or the eccentricity, as shown in Fig. 4. We found that for the 8 to $12 M_{\odot}$ progenitor, the pre-supernova orbit would require orbital periods in the range of $P_{\text{b,ini}} = 2000$ to $40\,000 \text{ d}$, while the Helium-star scenario with $M_{\text{p}} = 2.4$ to $4.0 M_{\odot}$ has compatible post-supernova orbits for $P_{\text{b,ini}} = 3000$ to $56\,000 \text{ d}$.

As a result of the low natal kick velocities, the velocity imparted on the post-supernova binary centre-of-mass is also low. The formalism by Brandt & Podsiadlowski (1995) predicts system velocities of $v_{\text{sys}} = 25$ to 45 km s^{-1} for a $10 M_{\odot}$ neutron star progenitor in a 1500 d pre-supernova orbit for the range of kick velocities in which the binary remains bound. These velocities decrease for lower mass neutron star progenitors and wider pre-supernova orbits.

6. Discussion and conclusions

The LOFAR timing observations of PSR J0210+5845 reveal large deviations from typical spin-down behaviour of isolated pulsars that can be modelled by a spin frequency and a spin frequency derivative. We argue that these deviations are caused by binary motion of the pulsar in a wide, as yet unresolved, orbit around the B6 V star 2MASS J02105640+5845176. This identification of 2MASS J02105640+5845176 as the binary companion of PSR J0210+5845 is based on the coincidence in celestial position, as well as the distance between the star and the pulsar, and the low probability for this coincidence to be due to random chance.

The properties of PSR J0210+5845, its B6 V binary companion, the orbital properties of this system and its location near the Galactic plane ($l = 133^{\circ}10$, $b = -2^{\circ}54$) are consistent to those of high-mass binary pulsars. With this identification, PSR J0210+5845 becomes the seventh system with this classification, i.e. non-recycled pulsars ($P > 0.01 \text{ s}$) with main-sequence star binary companions with masses in excess of $M_{\odot} >$

$1 M_{\odot}$ (Manchester et al. 2005). Compared to the other systems, PSR J0210+5845 stands out primarily due to the low mass of its binary companion. For those systems where companion masses have been reliably measured, the lowest mass is around $\sim 8 M_{\odot}$ (Table 1), while for the companion of PSR J0210+5845, we determined a mass of 3.5 to $3.8 M_{\odot}$. Similarly, among the high-mass X-ray binaries with measured masses, the lowest masses are around $\sim 8 M_{\odot}$ (from the HMXB catalogue by Fortin et al. 2023). The spin frequency derivatives determined from the timing of PSR J0210+5845 constrain the orbit to be wide ($P_{\text{b}} = 34$ to 88 yr) with a moderate eccentricity of $e = 0.39$ to 0.56 . Of the high-mass binary pulsars, only PSR J2032+4127 is in a wide orbit of 46 yr , though with a higher eccentricity of $e = 0.96$ (Lyne et al. 2015). All other systems have orbital periods below 2000 d .

Due to the low mass of the companion, we found that for the binary to remain bound after the supernova explosion that formed PSR J0210+5845, a low velocity, retrograde natal kick is required ($v_{\text{kick}} < 96 \text{ km s}^{-1}$). This is true for both the direct collapse of a $> 8 M_{\odot}$ neutron star progenitor as well as the collapse of a Helium star.

Low natal kicks of a few tens of km s^{-1} are commonly attributed to electron-capture supernovae, where the rapid explosion does not allow for asymmetries to develop (e.g. Podsiadlowski et al. 2004; Gessner & Janka 2018). The progenitor mass range in which electron-capture supernovae occur is uncertain but estimated between 8 and $10 M_{\odot}$. Recently, Stevenson et al. (2022) have postulated that electron-capture supernovae would create non-recycled pulsars in wide ($P_{\text{b}} \gtrsim 10^4 \text{ d}$) and moderately eccentric ($e \sim 0.7$) orbits. Their population synthesis predicts a distribution of post-supernova orbital periods and eccentricities matching the observed properties of PSR J0210+5845. Therefore, PSR J0210+5845 is a possible candidate for this formation scenario.

Although in traditional Fe core-collapse supernovae, large natal kicks of hundreds of km s^{-1} are predicted to be more common (Janka 2017, and references therein), observations show that lower natal kicks below 60 km s^{-1} are still possible (Verbunt et al. 2017). Due to the broader range of progenitor masses leading to a core-collapse supernova that produces a neutron star (Smartt 2009), this scenario is not to be disregarded.

The wide post-supernova orbit places constraints on the pre-supernova orbit, which we found requires to also be wide, with orbital periods ranging from 2000 to $56\,000 \text{ d}$. This would argue against the formation scenario in which an episode of mass transfer between the neutron star progenitor and the binary companion removes the envelope of the progenitor, allowing it to explode as a Helium star. First, the current low mass of the companion does not allow the neutron star progenitor to have accreted much matter, and second, the wide pre-supernova orbit is not expected in this scenario where mass-transfer is required. However, through calculations of angular momentum pre- and post-interaction and assuming no accretion by the companion, we found that under the ideal assumption of isotropic mass loss (e.g. see Pols & Marinus 1994), orbital periods exceeding 4000 d are achievable for a Helium star.

The orbital parameters indicate that the upcoming periastron passage is between 2030 and 2034. Continued timing observations around that time will significantly improve the orbital constraints. During periastron passage, the distance between the binary components is predicted to be $11.7^{+5.0}_{-1.5} \text{ AU}$, which, using the approximation from Eggleton (1983) and assuming a mass ratio of $1.4/3.6$, gives a Roche lobe radius of $R_{\text{L}} = 756^{+325}_{-101} R_{\odot}$ (Eggleton 1983). Comparatively, a $3.6 M_{\odot}$ star has an approximate ra-

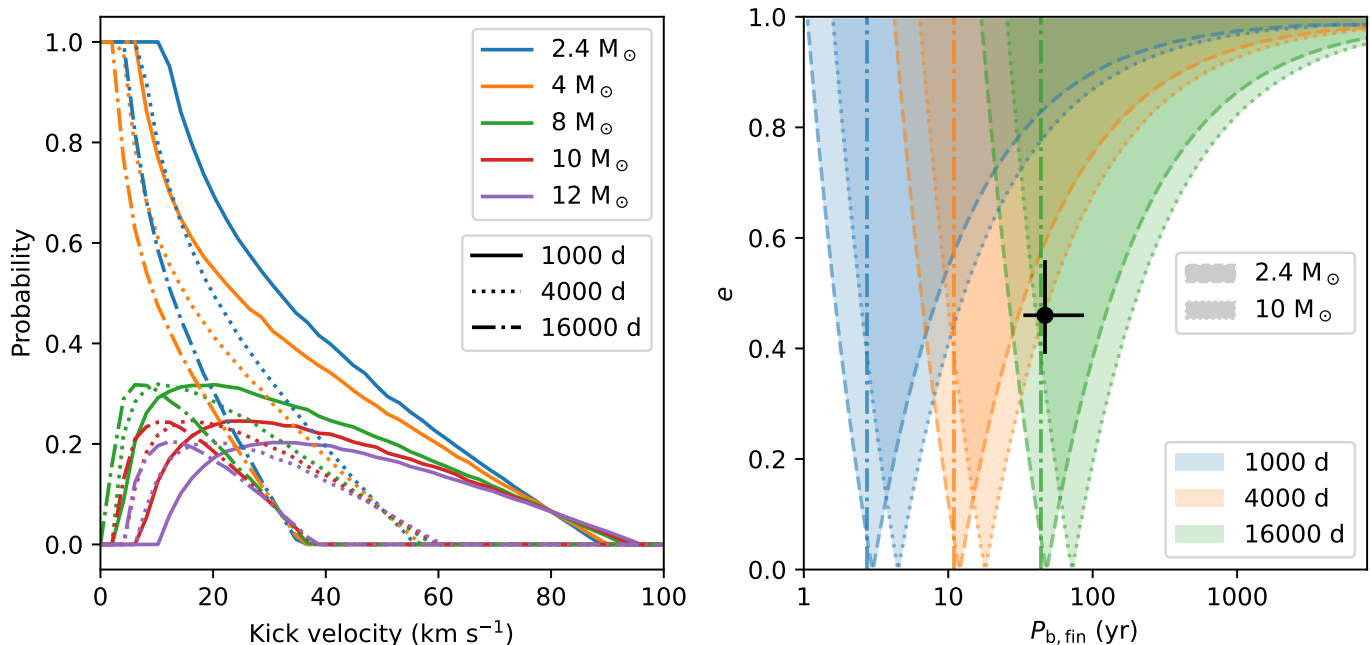


Fig. 4. Results from supernova kick simulations. The left-hand panel shows the probability that the post-supernova binary remains bound as a function of kick velocity. These probabilities were computed with isotropic kicks for a range of pre-supernova primary masses for a Helium-star progenitor of 2.4 and 4 M_{\odot} and direct supernova explosions of 8, 10, and 12 M_{\odot} progenitors as well as pre-supernova orbital periods of 1000, 4000, and 16 000 d. The right-hand panel shows the resulting post-supernova orbital period $P_{b,fin}$ and eccentricity for a range of pre-supernova masses and orbital periods. The dash-dotted vertical lines indicate the pre-supernova orbital periods with the wedges the resulting post-supernova parameters. The orbital constraints for PSR J0210+5845 are shown in black with error bars.

dus of $2.6 R_{\odot}$ (Demircan & Kahraman 1991), which indicates that there will be no Roche-lobe overflow.

At the nominal distance of 2.5 kpc, the observed proper motion of 2MASS J02105640+5845176 corresponds to a transverse velocity of 14.5 km s^{-1} . This velocity is the sum of the projected orbital velocity of the star around the binary centre-of-mass, the projected post-supernova system velocity of the binary centre-of-mass imparted on the system due to the supernova kick, and the projected component of any pre-supernova system velocity of the binary system. From the orbital constraints, we obtained a projected orbital velocity of the pulsar companion around the binary centre-of-mass of $3.1^{+0.5}_{-0.6} \text{ km s}^{-1}$. Assuming a random direction of the post-supernova system velocity, the projected component will be less than 22 km s^{-1} , indicating that the majority of the observed proper motion is due to the system velocity of the binary.

It remains to be seen if the orbital motion of the B6 V star around the centre-of-mass of the binary system can be detected by *Gaia*. The orbital constraints based on the observed spin frequency derivatives of PSR J0210+5845 indicate that the projected acceleration due to orbital motion is small, of order 0.02 mas yr^{-2} at a distance of 2.5 kpc, and the *Gaia* DR3 astrometric solution for position, proper motion and parallax reports no astrometric excess noise (Gaia Collaboration et al. 2023).

It has been proposed that numerous radio pulsars that are considered to be isolated, might in fact belong to exceptionally wide binary systems. Jones et al. (2023) estimate that approximately 30% of seemingly isolated pulsars with a measured \dot{f} could hide a binary with orbital period < 1000 years. In this paper, we have demonstrated that even in these highly separated systems, the orbital motion of the pulsar can be measured through higher-order frequency derivatives.

Acknowledgements. This paper is based (in part) on data obtained with the International LOFAR Telescope (ILT) under project codes LC9_023, LC9_041, LT10_015 and LT14_005. LOFAR (van Haarlem et al. 2013) is the Low Frequency Array designed and constructed by ASTRON. It has observing, data processing, and data storage facilities in several countries, that are owned by various parties (each with their own funding sources), and that are collectively operated by the ILT foundation under a joint scientific policy. The ILT resources have benefited from the following recent major funding sources: CNRS-INSU, Observatoire de Paris and Université d’Orléans, France; BMBF, MIWF-NRW, MPG, Germany; Science Foundation Ireland (SFI), Department of Business, Enterprise and Innovation (DBEI), Ireland; NWO, The Netherlands; The Science and Technology Facilities Council, UK; Ministry of Science and Higher Education, Poland. This research was made possible by support from the Dutch National Science Agenda, NWA Startimpuls – 400.17.608. IVY and JC acknowledge support by the Spanish Ministry of Science under grant PID2020-120323GB-I00. The INT is operated on the island of La Palma by the Isaac Newton Group of Telescopes in the Spanish Observatorio del Roque de los Muchachos of the Instituto de Astrofísica de Canarias.

References

- Aharonian, F., Akhperjanian, A. G., Aye, K. M., et al. 2005, *A&A*, 442, 1
 Anders, F., Khalatyan, A., Chiappini, C., et al. 2019, *A&A*, 628, A94
 Anders, F., Khalatyan, A., Queiroz, A. B. A., et al. 2022, *A&A*, 658, A91
 Andersen, B. C., Fonseca, E., McKee, J. W., et al. 2023, *ApJ*, 943, 57
 Arzoumanian, Z., Nice, D. J., Taylor, J. H., & Thorsett, S. E. 1994, *ApJ*, 422, 671
 Baileer-Jones, C. A. L., Rybizki, J., Fouesneau, M., Demleitner, M., & Andrae, R. 2021, *AJ*, 161, 147
 Bassa, C. G., Bricken, W. F., Nelemans, G., et al. 2011, *MNRAS*, 412, L63
 Bassa, C. G., Janssen, G. H., Karuppusamy, R., et al. 2016, *MNRAS*, 456, 2196
 Bell, J. F., Bessell, M. S., Stappers, B. W., Bailes, M., & Kaspi, V. M. 1995, *ApJ*, 447, L117
 Bellm, E. C., Kulkarni, S. R., Graham, M. J., et al. 2019, *PASP*, 131, 018002
 Brandt, N. & Podsiadlowski, P. 1995, *MNRAS*, 274, 461
 Bressan, A., Marigo, P., Girardi, L., et al. 2012, *MNRAS*, 427, 127
 Chen, X., Wang, S., Deng, L., et al. 2020, *ApJS*, 249, 18
 Chen, Y., Bressan, A., Girardi, L., et al. 2015, *MNRAS*, 452, 1068
 Chen, Y., Girardi, L., Bressan, A., et al. 2014, *MNRAS*, 444, 2525

- Cordes, J. M. & Lazio, T. J. W. 2002, astro-ph/0207156
- Demircan, O. & Kahraman, G. 1991, Ap&SS, 181, 313
- Eggleton, P. P. 1983, ApJ, 268, 368
- Eldridge, J. J., Izzard, R. G., & Tout, C. A. 2008, MNRAS, 384, 1109
- Fedurco, M., Paunzen, E., Hümmerich, S., Bernhard, K., & Parimucha, Š. 2020, A&A, 633, A122
- Fortin, F., García, F., Simaz Bunzel, A., & Chaty, S. 2023, A&A, 671, A149
- Gaia Collaboration, Vallenari, A., Brown, A. G. A., et al. 2023, A&A, 674, A1
- Gessner, A. & Janka, H.-T. 2018, ApJ, 865, 61
- Green, G. M., Schlafly, E., Zucker, C., Speagle, J. S., & Finkbeiner, D. 2019, ApJ, 887, 93
- Henden, A. A., Levine, S., Terrell, D., & Welch, D. L. 2015, in American Astronomical Society Meeting Abstracts, Vol. 225, American Astronomical Society Meeting Abstracts #225, 336.16
- Hills, J. G. 1983, ApJ, 267, 322
- Hobbs, G., Lyne, A. G., & Kramer, M. 2010, MNRAS, 402, 1027
- Hotan, A. W., van Straten, W., & Manchester, R. N. 2004, PASA, 21, 302
- Hynes, R. I. 2002, A&A, 382, 752
- Janka, H.-T. 2017, ApJ, 837, 84
- Johnston, S., Manchester, R. N., Lyne, A. G., Nicastro, L., & Spyromilio, J. 1994, MNRAS, 268, 430
- Jones, M. L., Kaplan, D. L., McLaughlin, M. A., & Lorimer, D. R. 2023, ApJ, 951, 20
- Joshi, K. J. & Rasio, F. A. 1997, ApJ, 479, 948
- Kaspi, V. M., Bailes, M., Manchester, R. N., Stappers, B. W., & Bell, J. F. 1996, Nature, 381, 584
- Klencki, J., Istrate, A., Nelemans, G., & Pols, O. 2022, A&A, 662, A56
- Kondratiev, V. I., Verbiest, J. P. W., Hessels, J. W. T., et al. 2016, A&A, 585, A128
- Lorimer, D. R., Faulkner, A. J., Lyne, A. G., et al. 2006, MNRAS, 372, 777
- Luo, J., Ransom, S., Demorest, P., et al. 2021, ApJ, 911, 45
- Lyne, A. G., Stappers, B. W., Keith, M. J., et al. 2015, MNRAS, 451, 581
- Madsen, E. C., Stairs, I. H., Kramer, M., et al. 2012, MNRAS, 425, 2378
- Manchester, R. N., Hobbs, G. B., Teoh, A., & Hobbs, M. 2005, AJ, 129, 1993
- Matzner, C. D. & McKee, C. F. 1999, ApJ, 510, 379
- Morello, V., Barr, E. D., Cooper, S., et al. 2019, MNRAS, 483, 3673
- Munari, U., Sordo, R., Castelli, F., & Zwitter, T. 2005, A&A, 442, 1127
- Nice, D. J. & Taylor, J. H. 1995, ApJ, 441, 429
- Pecaut, M. J. & Mamajek, E. E. 2013, ApJS, 208, 9
- Podsiadlowski, P., Langer, N., Poelarends, A. J. T., et al. 2004, ApJ, 612, 1044
- Pols, O. R. & Marinus, M. 1994, A&A, 288, 475
- Queiroz, A. B. A., Anders, F., Chiappini, C., et al. 2020, A&A, 638, A76
- Queiroz, A. B. A., Anders, F., Santiago, B. X., et al. 2018, MNRAS, 476, 2556
- Sanidas, S., Cooper, S., Bassa, C. G., et al. 2019, A&A, 626, A104
- Schlaflly, E. F. & Finkbeiner, D. P. 2011, ApJ, 737, 103
- Shannon, R. M., Johnston, S., & Manchester, R. N. 2014, MNRAS, 437, 3255
- Shklovskii, I. S. 1970, Soviet Ast., 13, 562
- Skrutskie, M. F., Cutri, R. M., Stiening, R., et al. 2006, AJ, 131, 1163
- Smartt, S. J. 2009, ARA&A, 47, 63
- Stevenson, S., Willcox, R., Vigna-Gómez, A., & Broekgaarden, F. 2022, MNRAS, 513, 6105
- Tan, C. M., Bassa, C. G., Cooper, S., et al. 2020, MNRAS, 492, 5878
- Tang, J., Bressan, A., Rosenfield, P., et al. 2014, MNRAS, 445, 4287
- Tauris, T. M., Kramer, M., Freire, P. C. C., et al. 2017, ApJ, 846, 170
- van der Wateren, E., Bassa, C. G., Cooper, S., et al. 2023, A&A, 669, A160
- van Haarlem, M. P., Wise, M. W., Gunst, A. W., et al. 2013, A&A, 556, A2
- van Straten, W. & Bailes, M. 2011, PASA, 28, 1
- Verbunt, F., Igoshev, A., & Cator, E. 2017, A&A, 608, A57
- Waelkens, C. 1991, A&A, 246, 453
- Wang, N., Johnston, S., & Manchester, R. N. 2004, MNRAS, 351, 599
- Woosley, S. E., Heger, A., & Weaver, T. A. 2002, Reviews of Modern Physics, 74, 1015
- Xiang, M., Rix, H.-W., Ting, Y.-S., et al. 2022, A&A, 662, A66
- Xiang, M., Ting, Y.-S., Rix, H.-W., et al. 2019, ApJS, 245, 34
- Yao, J. M., Manchester, R. N., & Wang, N. 2017, ApJ, 835, 29